Experimental and numerical study of band-broadening effects associated with analyte transfer in microfluidic devices for spatial two-dimensional liquid chromatography created by additive manufacturing

Adamopoulou, T.; Nawada, S.; Deridder, S.; Wouters, B.; Desmet, G.; Schoenmakers, P.J.

DOI
10.1016/j.chroma.2019.03.041

Publication date
2019

Document Version
Final published version

Published in
Journal of Chromatography A

License
CC BY

Journal of Chromatography A, 1598 (2019) 77–84

Contents lists available at ScienceDirect

Journal of Chromatography A

journal homepage: www.elsevier.com/locate/chroma

Experimental and numerical study of band-broadening effects associated with analyte transfer in microfluidic devices for spatial two-dimensional liquid chromatography created by additive manufacturing☆

Theodora Adamopoulou[a,*], Suhas Nawada[a], Sander Deridder[b], Bert Wouters[a], Gert Desmet[b], Peter J. Schoenmakers[a]

[a] Universiteit van Amsterdam, Van' t Hoff Institute for Molecular Sciences, Science Park 904, 1098 XH, Amsterdam, the Netherlands
[b] Vrije Universiteit Brussel, Department of Chemical Engineering, Pleinlaan 2, B-1050, Brussels, Belgium

ARTICLE INFO

Article history:
Received 30 November 2018
Received in revised form 19 March 2019
Accepted 20 March 2019
Available online 22 March 2019

Keywords:
Spatial chromatography
Additive manufacturing
Computational fluid dynamics
LC × LC
Band broadening
Analyte transfer

ABSTRACT

Conventional one-dimensional column-based liquid chromatographic (LC) systems do not offer sufficient separation power for the analysis of complex mixtures. Column-based comprehensive two-dimensional liquid chromatography offers a higher separation power, yet suffers from instrumental complexity and long analysis times. Spatial two-dimensional liquid chromatography can be considered as an alternative to column-based approaches. The peak capacity of the system is ideally the product of the peak capacities of the two dimensions, yet the analysis time remains relatively short due to parallel second-dimension separations. Aspects affecting the separation efficiency of this type of systems include flow distribution to homogeneously distribute the mobile phase for the second-dimension (^{2}D) separation, flow confinement during the first-dimension (^{1}D) separation, and band-broadening effects during analyte transfer from the ^{1}D separation channel to the ^{2}D separation area.

In this study, the synergy between computational fluid dynamics (CFD) simulations and rapid prototyping was exploited to address band broadening during the ^{2}D development and analyte transfer from ^{1}D to ^{2}D. Microfluidic devices for spatial two-dimensional liquid chromatography were designed, simulated, 3D-printed and tested. The effects of presence and thickness of spacers in the ^{2}D separation area were addressed and leaving these out proved to be the most efficient solution regarding band broadening reduction. The presence of a stationary-phase material in the ^{1}D channel had a great effect on the analyte transfer from the ^{1}D to the ^{2}D and the resulting band broadening. Finally, pressure limit of the fabricated devices and printability are discussed.

1. Introduction

Analytical chemists are increasingly confronted with samples of high complexity from many different fields (*e.g.* life science, food, environmental, and materials). This creates a need for highly selective methods for analysing specific components and for advanced, comprehensive methods to fully characterize the samples. Two-dimensional separation methods, such as comprehensive two-dimensional liquid chromatography (LC × LC), are among the most powerful methods for separating complex samples, prior to detecting and characterizing individual components using, for example, mass spectrometry [1]. This is reflected in the many applications of LC × LC for separating samples as diverse as proteins [2–4], polymers [5–7], phenols in food [8–10], and wastewater [11]. Usually, LC × LC is performed in a column-based format. The sample is first separated in a first-dimension column, the effluent of which is divided in many fractions, which are sequentially transferred to a second-dimension column for further separation. Column-based LC × LC is now well established and suitable instrumentation and software are available commercially. Many different retention mechanisms can be combined [12] and LC × LC can be readily coupled with mass spectrometry for on-line characterization of the separated compounds. By using state-of-the-art (ultra-)

☆ Selected paper from the 47th International Symposium on High Performance Liquid Phase Separations and Related Techniques (HPLC2018), July 29-August 2, 2018, in Washington, DC, USA.

* Corresponding author.
E-mail address: t.adamopoulou@uva.nl (T. Adamopoulou).

https://doi.org/10.1016/j.chroma.2019.03.041

high-performance LC technology in both dimensions and by combining two very different ("orthogonal") mechanisms, very high peak capacities can be realized. By matching the separation mechanisms with the properties of the sample ("sample dimensions" [13],) structured, readily interpretable chromatograms may be obtained [14].

An alternative format is "spatial" LC × LC. Instead of eluting compounds from a column at a specific time ("time-based"), analytes are characterized by the position to which they have migrated in the separation medium ("space-based"). In two-dimensional spatial LC × LC, the analytes are subsequently moved from their characteristic positions in a perpendicular direction in a second-dimension separation, either to a new position in the two-dimensional plane (^{x}LC × ^{x}LC) [15] or by elution (^{x}LC × ^{t}LC) [16,17]. Different conditions (retention mechanisms) are used in the two dimensions [18]. A typical example is 2D-poly(acryl amide) gel electrophoresis (2D-PAGE), where iso-electric focussing is used in the first dimension, followed by gel electrophoresis in the second dimension [19,20]. The LC equivalent of 2D-PAGE, two-dimensional thin-layer chromatography (2D-TLC) has not yet developed into a truly high-performance technique, which would require high-pressure operation. Fundamentally, because all second-dimension separations are performed simultaneously, spatial LC × LC may outperform "temporal", column-based LC × LC in terms of peak capacity per unit time. These advantages are greatly amplified when considering a third dimension [21]. Comprehensive three-dimensional liquid chromatography (spatial 3D-LC) may potentially yield peak capacities approaching one-million in a reasonable time and at moderate pressures [22]. Therefore, it is highly relevant to develop efficient spatial chromatography devices.

In a recently described 2D spatial separation device [23], the analytes are first separated in a first dimension (^{1}D) channel and then all transferred simultaneously to a second-dimension (^{2}D) separation space. A ^{2}D mobile phase flow distributor was used to homogenously flush the analytes from the ^{1}D channel into the second dimension without undoing the first separation. In this format the flow field and mass transfer from the ^{1}D channel to ^{2}D regions can greatly affect the separation efficiency. Additionally, any fabrication inaccuracy could prove detrimental to the operation of the device.

The development of microfluidic devices is an iterative process of designing and prototyping. Designs that appear satisfactory are prototyped and tested. The resulting experimental data on their performance can be used to enhance the design further. By using computational fluid dynamics (CFD) initial designs can be tested, while avoiding practical obstacles, yielding data that are otherwise difficult or sometimes even impossible to obtain. Because microfluidic devices feature numerous key parameters that affect critical decisions in the design process, prototyping can be a time-consuming and expensive process [24]. Some previous contributions from CFD studies involved flow distribution and selecting the number of channels in the second dimension [25–27].

In this study, the synergy between computational simulations and rapid prototyping was exploited to create and test novel microfluidic devices for spatial two-dimensional liquid chromatography. The geometries examined consisted of three main parts, *viz.* the flow distributor for the ^{2}D mobile phase, the ^{1}D channel and the ^{2}D area (*i.e.* flat bed or 16 discrete channels). As a first step, CFD was used to study the flow through the ^{2}D flow distributor and mass transfer from the ^{1}D to the ^{2}D channels. Additionally, devices were simulated with and without (particulate or monolithic) separation media in the ^{1}D channel. The transfer of a mixture of dye and water from the ^{1}D channel to the ^{2}D area was simulated and the method of moments was used to calculate the ^{2}D band variance. After the computational evaluation of various designs was completed, a smaller selection of suitable devices were 3D-printed *via* a high-resolution digital-light-processing (DLP) approach and band-broadening effects were compared between simulated and printed devices without stationary-phase material. Finally, the pressure limit of these 3D-printed devices was investigated.

Table 1
Different design types for the examined microfluidic devices as characterized by i) the internal diameter of distributor channels, ii) the presence or absence of a stationary phase in the ^{1}D channel, and iii) the spacer thickness between the discrete channels in the ^{2}D area.

Type	Flow-distributor channels (I.D., mm)	Stationary phase in ^{1}D channel	Spacer thickness for ^{2}D channels (mm)
I	0.3	No	No spacers
II	0.3	No	0.5
III	0.3	No	0.1
IV	0.3	Yes	No spacers
V	0.3	Yes	0.5
VI	0.3	Yes	0.1
VII	0.6	No	0.5
VIII	0.7	No	0.5
IX	0.8	No	0.5
X	1.0	No	0.5
XI	1.0	No	0.1
XII	1.0	No	No spacers

2. Materials and methods

2.1. Chemicals

The methacrylate-based resin Asiga PlasClear V2 was purchased from 3DXS (Erfurt, Germany). 2-Propanol was obtained from Biosolve (Valkenswaard, The Netherlands). PME Natural Food Color (Red) was obtained from Knightsbridge PME (Enfield, United Kingdom).

2.2. Computational fluid dynamics (CFD) studies

For all CFD simulations, ANSYS Workbench Fluids and Structures Academic package (versions 16.2–17.2) was used (ANSYS, Canonsburg, PA, USA). All simulations were conducted using the Fluent solver. All types of devices studied were discretized in a similar manner with ANSYS Meshing. In regions where the highest velocity and concentration gradients were expected, smaller sized cells were used, to increase the accuracy of the computations. These regions were expected to be located near the walls of the distributor and the ^{2}D area (because of the no-slip boundary condition) and throughout the entire ^{1}D channel (because of the large change in cross-sectional area from the distributor to the ^{1}D channel). More specifically, the distributor was meshed with an unstructured tetrahedral grid with inflation layers (=length with gradually growing cell size) on the distributor walls, the ^{1}D channel was meshed with an unstructured tetrahedral grid with fixed maximum cell size and the ^{2}D area was meshed with a structured hexahedral grid with smaller cells near the walls. The number of elements in all cases was around 2 500 000. All cases were solved for flow [28] and species-transport. In the latter, Fick's law for diffusion applies [29]. An example of the agreement between ANSYS and the analytical Aris solution can be found in the work of Gzil et al. [30].

A total of ten variants of the devices were examined, as summarized in Table 1 and illustrated in Fig. 1. The key distinguishing factor between these designs was the nature of the ^{2}D area, either being a uniform flat bed or consisting of 16 discrete channels separated by spacers. Two types of spacers were studied (*i.e.* 0.1 or 0.5 mm thickness) and all types had the same flow distributor format composed of cylindrical channels with an internal diameter varying from 0.3 to 1.0 mm with 90° angle T-junctions. These

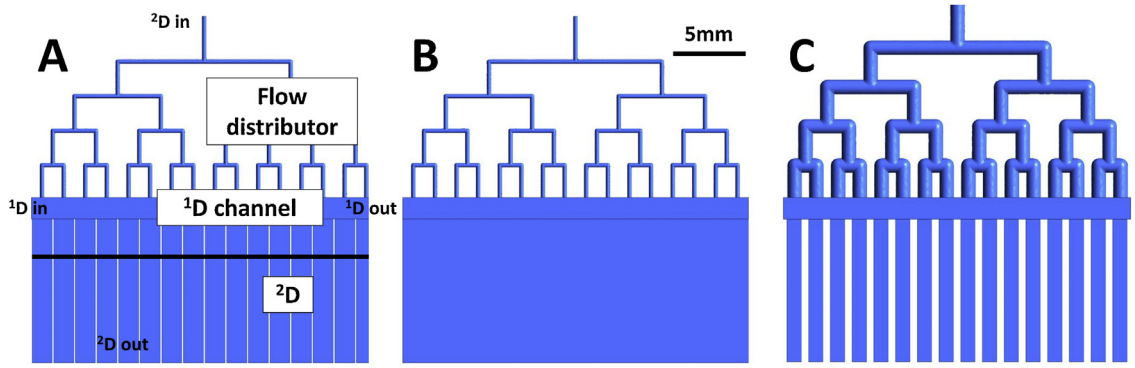

Fig. 1. Typical spatial 2D-LC device with 3 main parts, viz. the flow distributor for the second-dimension separation (^{2}D) mobile phase, the first-dimension separation (^{1}D) channel and the second-dimension separation (^{2}D) area. The line in the ^{2}D space represents a control line used for data extraction. Figure A shows the geometry used in types III and VI, B shows the geometry used in types I and IV, and C shows the geometry used in type X.

dimensions took into consideration the best-possible resolution of the DLP 3D-printer used in this research.

Simulations were conducted for both an empty ^{1}D channel and for a ^{1}D channel containing a stationary-phase material. The porous zone is not physically present and in order to approximate its effect the superficial-velocity porous formulation is applied, where the mixture velocities are calculated based on the flow rate in a porous region. The porosity is assumed to be isotropic and porosity is not taken into account for the calculation of diffusion terms in the transport equations. The examined types with an empty ^{1}D channel are representative of 2D separation devices previously reported in literature, in which isoelectric focusing was used as the ^{1}D separation method [31,32]. The types simulated for a ^{1}D channel with a stationary phase represented the presence of an organic polymer monolith. This presence was mimicked by treating the ^{1}D channel as a porous zone with permeability 1.7 10^{-13} m^2, a typical value for polymer monoliths [33]. The dimensions of the ^{1}D channel were 24 × 1.5 × 1.5 mm ($L \times w \times h$). The process of ^{1}D injection was not included in this study to eliminate any variations caused by the ^{1}D injection and to reduce the computational cost. Instead, a fully-filled ^{1}D channel was imposed during the initialization step, containing a mixture of 1% (w/w) dye in water. For the ^{2}D simulations, water was introduced through the flow distributor. During the transfer to the ^{2}D, the ^{1}D inlet and outlet were closed. The inlet boundary condition was adjusted in all three types to achieve an average velocity of 0.98 mm/s in the ^{2}D area. The dimensions of the ^{2}D area were 24 × 10 × 1.5 mm ($L \times w \times h$) for the cases without spacers, 23.5 × 10 × 1.5 mm ($L \times w \times h$) for the cases with spacers of 0.5 mm thickness and 23.9 × 10 × 1.5 mm ($L \times w \times h$) for the cases with spacers of 0.1 mm thickness.

To determine the suitability of the design related to the spacer thickness in the ^{2}D area, the method of moments was used to calculate the band variance. The calculation of the moments and variance is reflected by Eqs. (1)–(4).

$$\mu(0) = \int_0^\infty c(x)\,dx \tag{1}$$

$$\mu'(1) = \frac{\int_0^\infty xc(x)\,dx}{\mu(0)} \tag{2}$$

$$\mu'(2) = \frac{\int_0^\infty x^2 c(x)\,dx}{\mu(0)} \tag{3}$$

$$\sigma^2 = \mu^{'}(2) - \mu'(1)^2 \tag{4}$$

In Eqs. (1)–(4), $\mu(0)$ is the zeroth, $\mu'(1)$ the first and $\mu'(2)$ the second moment, σ^2 is the variance and c(x) corresponds to the transversally averaged concentration of dye across the ^{2}D zone from x to x + dx as calculated per time step. In this way, the transfer of the analytes from the ^{1}D channel to the ^{2}D area could be observed. During the grid independence study the maximum difference for pressure and for the velocity component of the direction of the flow was 0.0023% and 0.0021%, respectively. The time-step choice was made in respect with the minimum cell volume and the chosen velocity.

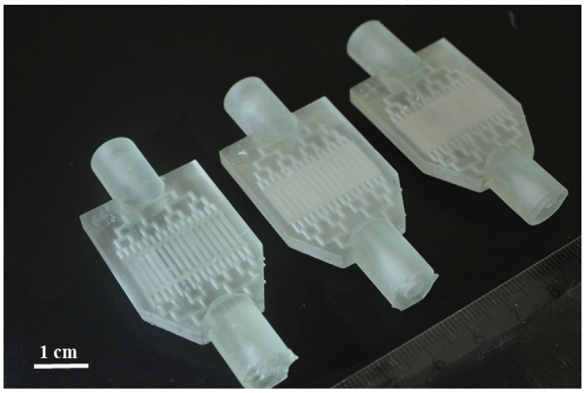

Fig. 2. Photographs of 3D-printed devices used for assessing flow profiles. Devices of type X (left), type XI (middle) and type XII (right) without stationary-phase material.

2.3. 3D-Printing of microfluidic devices

Microfluidic devices were designed using SOLIDWORKS (Dassault Systèmes SOLIDWORKS, Waltham, MA, USA) and Autodesk Inventor (Autodesk, San Rafael, CA, USA). Devices (Fig. 2; *vide infra* Figs. 6 and 8) were fabricated through digital light processing (DLP) using an Asiga Pico 2 HD 3D-printer (Asiga Germany, Erfurt, Germany).

The design was converted to STL format, loaded through the 3D printer software interface (Asiga Composer), and printing orientation and settings were optimized for high resolution and fabrication time The devices shown in Fig. 2 were printed vertically to the build platform of the printer, while the devices used for pressure testing (Fig. 8) were printed horizontally to the build platform. This placement difference had an effect on the appearance of the devices where in Fig. 2 the devices have a “milky” appearance while the top layer of the device in Fig. 8 is more shiny. After 3D-printing, devices were post-processed by sonication and flushing of channels with 2-propanol and nitrogen gas to remove any uncured resin. Finally, parts were placed in a Pico Flash UV chamber (type 87 DR-301C, 36 W, 365 nm; 3DXS, Erfurt, Germany) and cured for 30 min. To make the devices connectable, straight threads (#10-32 UNC,

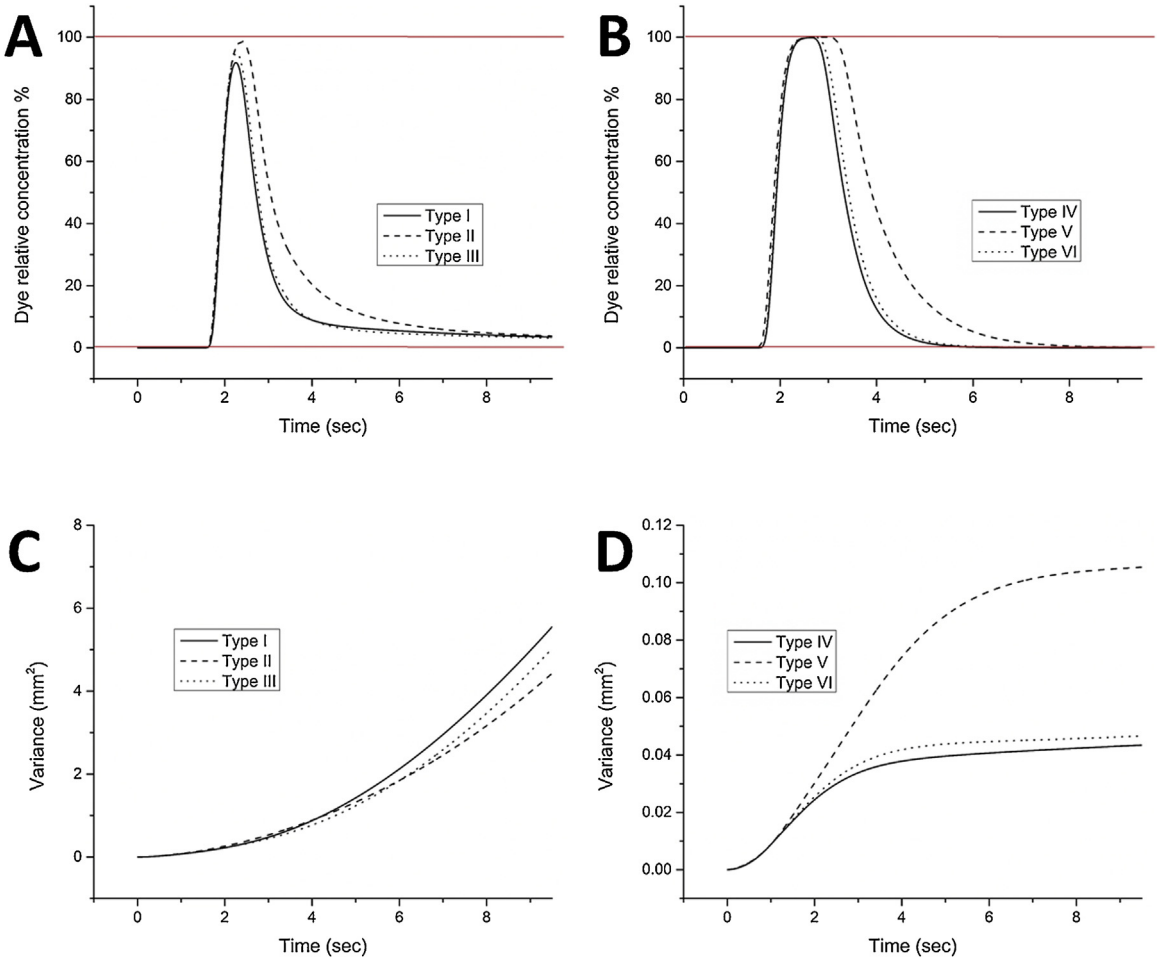

Fig. 3. Relative dye concentration (A&B) recorded at a control plane close to the transition zone (3 mm from the ^{1}D to ^{2}D interface zone towards the ^{2}D outlet) and band variance along the ^{2}D direction (C&D) for devices with an empty ^{1}D channel, *i.e.* type I-III (A&C) and for devices with a ^{1}D channel with a stationary phase *i.e.* types IV–VI (B&D). Solid line corresponds to the flat-bed ^{2}D area, dotted line to ^{2}D channels with 0.1 mm spacer thickness, and dashed line corresponds to ^{2}D channels with 0.5 mm spacer thickness.

major diameter 4.83 mm, 95 thread pitch 0.794 mm) were created using a hand tap. A conical ferrule seat was 3D-printed to facilitate a leak-proof connection to the outlet of the device.

2.4. Evaluation of printed devices

To compare the performance in terms of dye flow profiles and band-broadening effects between simulated and printed devices, flow tests were conducted in printed devices that featured a flow distributor, a ^{1}D channel, a ^{2}D area and a flow collector. The devices were completely filled with 2-propanol and a mixture of red dye dissolved in 2-propanol (1%) was then injected through the distributor for flow visualization. The injection was realized with an injection valve, and the injection volume was less than 5% of the volume of the ^{2}D area. Flow profiles were recorded with a Canon EOS 1300D camera (Canon Inc., Tokyo, Japan). To quantitatively evaluate the performance of the devices, the red colour intensity was quantified along two horizontal (^{1}D direction) control lines at the beginning and end of the ^{2}D area and analysis was conducted using Mathematica (Wolfram, Champaign, IL, USA). Finally, the pressure limit of the printed devices was studied by increasing the flow rate until failure (*i.e.* breakage or leakage). For this purpose, devices with a flow distributor, an empty flat ^{2}D area and inlet and outlet connections were printed. Devices were connected to an LC-10 AD VP Shimadzu liquid-chromatography pump (Shimadzu, Kyoto, Japan) and the flow rate was gradually increased until failure while the pressure was recorded. All measurements were conducted (at least) in triplicates. Appropriate safety measures were taken to shield analysts from any possible spray of liquid or flying pieces of resin. Neither of these latter were encountered during the study.

3. Results and discussion

Various design aspects, which were thought to affect the performance of spatial two-dimensional liquid-chromatography devices, were assessed. As shown in Fig. 1, the examined devices consisted of three main parts, *viz.* (*i*) the flow distributor aimed to homogeneously distribute the mobile phase for the second-dimension (^{2}D) separation across (*ii*) the first-dimension (^{1}D) separation channel and (*iii*) the ^{2}D separation area (*i.e.* flat bed or 16 discrete channels). A separation in the described devices occurs by the following series of subsequent steps, *viz.* (*i*) sample injection and ^{1}D separation, while the ^{2}D inlet and outlet are closed, (*ii*) introduction of the mobile phase for the ^{2}D separation, while the ^{1}D inlet and outlet are closed, (*iii*) transfer of analytes from the ^{1}D channel to the ^{2}D area, and finally (*iv*) parallel separation of the entire content of the ^{1}D channel in the ^{2}D area. Detection can occur either *in-situ* (*e.g.* by confocal spectroscopy in a transparent device), on-line at the end of the ^{2}D area (*e.g.* by laser-induced fluorescence, LIF [19]), or offline *via* collection of the effluent (*e.g.* by immobilization on a substrate followed by matrix-assisted laser-desorption/ionization mass spectrometry, MALDI-MS [31]).

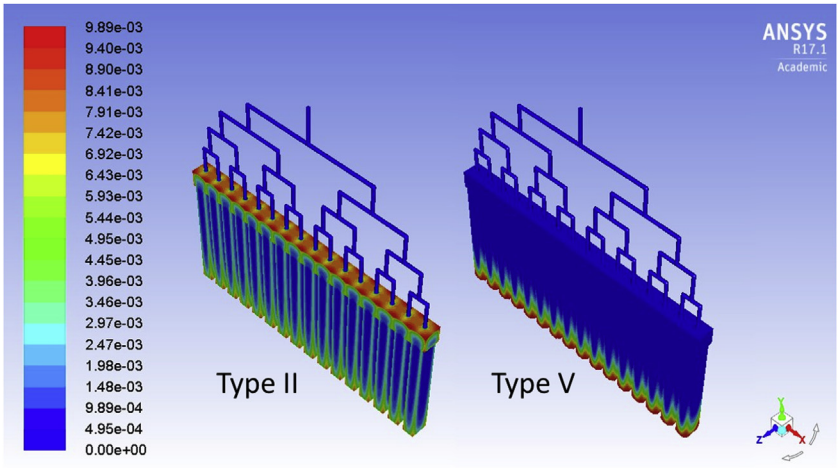

Fig. 4. Contour plots of mass fraction of dye in type II (left) and type V (right) devices after the ^{2}D injection of water for one device volume. Colour scale ranges from 0 (blue) to 9.89 10^{-3} (red) (For interpretation of the references to colour in this figure legend, the reader is referred to the web version of this article).

3.1. Computational fluid dynamics

3.1.1. Effect of ^{2}D geometry on band broadening

The first six device types described in Table 1 were compared in terms of band variance and relative dye concentration during transfer of dye from the ^{1}D channel to the ^{2}D area. In all types the initial state was a ^{1}D channel uniformly filled with a mixture of dye and water. Subsequently, water was introduced through the flow distributor, while the ^{1}D inlet and outlet were closed. As a result, the dye mixture in the ^{1}D channel was transferred to the ^{2}D area.

The relative dye concentration and the band variance recorded over time are shown in Fig. 3. Fig. 3A and B depict the band profiles recorded at a control plane close to the transition zone (3 mm from the ^{1}D to ^{2}D interface zone towards the ^{2}D outlet) for types I-III, with an empty ^{1}D channel, and types IV-VI, with a ^{1}D channel containing a stationary material, respectively. The open ^{1}D channels give rise to an initial sharp band, followed by a seemingly endless tail, indicative of the presence of stagnant areas in between flow lines from the distributor to the ^{2}D area. In case where stationary material is present in the ^{1}D channel the initial pulse is a bit broader, but all of the dye is washed from the ^{1}D channel within a few seconds. The corresponding band variances in the ^{2}D direction, calculated using Eqs. (1)–(4), are much higher (app. hundred-fold) in cases where there is no ^{1}D stationary-phase material (Fig. 3C) than in case of a ^{1}D channel containing a stationary-phase material (Fig. 3D). In case of an empty ^{1}D channel the band variance keeps increasing during the ^{2}D injection of one device volume, while it levels off in case of a ^{1}D channel containing a stationary material.

In Fig. 3A it can be observed that for the device types with an empty ^{1}D channel (types I–III) the dye concentration at the control plane remains significant, long after the band has moved towards the outlet. This implies that the dye remains present in the device after the transfer operation is meant to have ended. This is in accordance with the contour plot shown in Fig. 4 (left), where dye is seen to have remained in the ^{1}D channel after a full device volume of water has been flushed through. This incomplete dye transfer indicates poorly-permeated ("dead") zones in the ^{1}D channel. When comparing types containing stationary material in the ^{1}D channel (types IV-VI), it is interesting to note that types IV and VI, which represent a flat-bed ^{2}D area and one with discrete ^{2}D channels with the minimal 0.1 mm spacer thickness, respectively, show an almost identical, symmetrical dye-concentration profile. On the other hand, type V, which features discrete ^{2}D channels with 0.5 mm spacer thickness, gives rise to a broader, tailing dye-concentration profile, due to dead zones formed in front of these spacers.

3.1.2. Analyte transfer from ^{1}D channel to ^{2}D separation spaces

Fig. 4shows two examples of the dye plugs migrating to the end of the ^{2}D area for the type II (empty ^{1}D channel, discrete ^{2}D channels with 0.5 mm spacer thickness) and type V (^{1}D channel with stationary material, discrete ^{2}D channels with 0.5 mm spacer thickness) devices.

To study the issue of incomplete transfer of dye from the ^{1}D channel to the ^{2}D area caused by poorly-permeated zones in case of an empty ^{1}D channel, the effect of the internal diameter of the bifurcating distributor channels (*i.e.* 0.3, 0.6, 0.7, 0.8, and 1.0 mm) on the dye transfer was examined. Increasing the distributor channel diameter might decrease the size of the dead zones located in the ^{1}D channel between the distributor entry points. Types II and VII-X with an empty ^{1}D channel and a ^{2}D area consisting of discrete channels with 0.5 mm spacer thickness were selected for this study. The height and width of the ^{1}D channels (both 1.5 mm) and the height and width of the ^{2}D channels (1.5 mm and 1.0 mm, respectively), where kept constant in this study.

Fig. 5 A shows a histogram of the volume fractions of the binned mesh elements relative to the total ^{1}D channel volume based on the velocity magnitude from steady-state simulations on the device. Low local velocities indicate poorly-permeated dead zones in the ^{1}D channel. It is seen that narrow flow distributor channels cause dead zones in more than 10% of the total volume (left-hand side of Fig. 5A) and would therefore cause poor analyte transfer. Increasing the internal diameter clearly reduces the volume fraction of near-stagnant zones. The latter can be understood from the fact that the wider flow distributor channels lead to a larger fraction of ^{1}D channel that is readily swept by the incoming ^{2}D flow distributor flow.

Transient simulations mimicking analyte transfer with a dye flushed into the ^{2}D space were performed. In Fig. 5B the dye recovery after the band has transferred from the ^{1}D channel to the ^{2}D channels is shown. Ideally, 100% of the dye is recovered, but thus ideal situation is never reached because of the dead zones in the ^{1}D channel. The percentage of dye remaining in the ^{1}D channel is seen to decrease when the diameter of the distributor channel diameter increases from 0.3 to 1.0 mm. This is in accordance with the reduction of the dead zones observed in Fig. 5A. These results confirm the trends seen with the steady-state simulations (Fig. 5A), *i.e.* that larger diameter distributor channels facilitate better analyte transfer between the two dimensions.

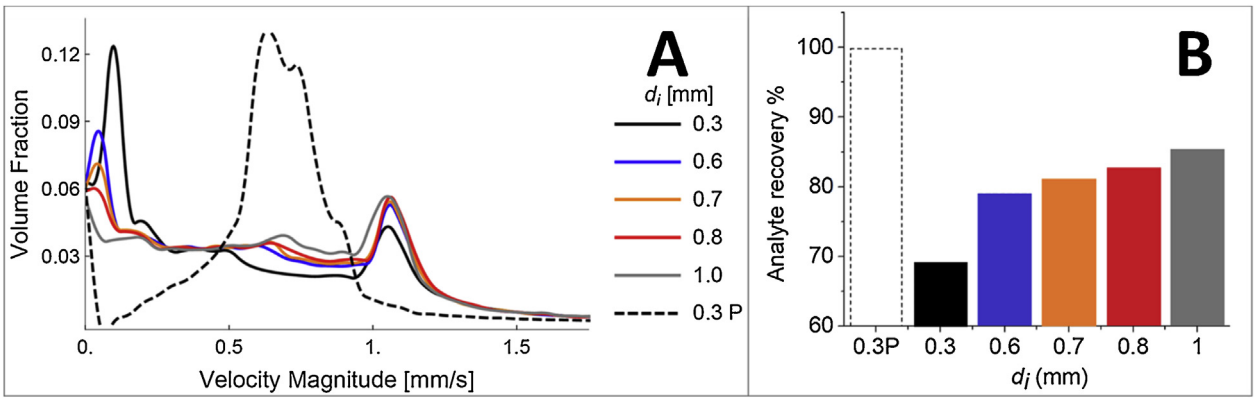

Fig. 5. A) Velocity distribution within the ^{1}D channel during transfer from the ^{1}D channel to ^{2}D region. The vertical axis displays the fraction of the total volume that exhibits a specific local velocity magnitude during a ^{2}D flushing step with a bin size of 5 μm for device types II, VII-X (solid lines) with empty ^{1}D channel and V (dashed line) with a ^{1}D channel with stationary-phase material. B) Calculated recovery of the dye solution at the ^{2}D outlet measured after flushing with one total device volume.

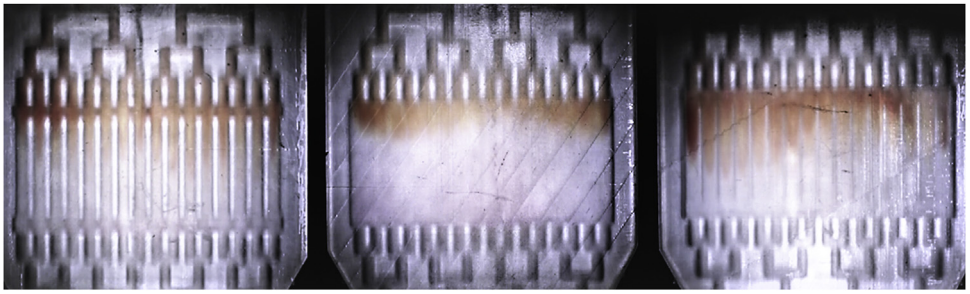

Fig. 6. Photographs of 3D-printed devices during flow testing, after the dye started entering the ^{2}D space. Devices of type X (left), type XII (middle) and type XI (right) without stationary-phase material.

Nevertheless, transferring under 90% of the analytes to the second-dimension region is far from ideal for effective 2D-LC separations. This can be mitigated by the presence of a stationary phase in the ^{1}D region, as illustrated in Figs. 4 and 5. As can be observed from case 0.3 P in Fig. 5, which incorporates a 0.3-mm flow-distributor and a porous ^{1}D channel, the flow resistance caused by the stationary phase ($5.6\ 10^{12}\ m^{-2}$) homogenizes the flow profile in the *y*-direction and results in a nearly complete (up to 99.8%) transfer to the ^{2}D space. However, a microfluidic device containing two different stationary phases can introduce a new set of practical challenges, such as analyte spill-over between the stationary phases. Therefore, novel analyte transfer solutions such as the Twist valve [34] may be necessary for achieving sufficient analyte transfer and consequently, high peak-capacities in spatial 2D-LC devices.

3.2. Experimental evaluation of 3D-Printed microfluidic devices

3.2.1. Flow profiles

After comparing a variety of microfluidic devices using CFD, a selection of devices was prototyped by high-resolution DLP 3D-printing. To study the effect of the ^{2}D geometries on flow profiles in the 3D-printed devices, a dye mixture was injected to the three examined types, as it is shown in Fig. 6 *viz.* a flat (undivided) ^{2}D bed and two types with discrete channels in the ^{2}D area. A drawing of the details of the in- and outlets to the ^{1}D channel has been added to the supplementary material (Fig. S1). This shows significant dead zones can be expected to develop, explaining (at least partly) the relatively wide zone injected in the ^{2}D in Fig. 6.

The band variance was calculated at 16 equidistant control points along two control lines parallel to the ^{1}D channel, one at the start and one at the end of the ^{2}D area. The variance at the starting points was then subtracted from the variance at the points near the end of the ^{2}D area. In Fig. 7A when observing only the variance calculated at the starting points the highest value corresponds to the type with discrete channels with 0.5 mm spacer thickness and the lowest to the case with no spacers. In Fig. 7B, the difference in variance between the two control lines per point is presented, with the largest contribution to band variance observed in the type with discrete channels with 0.1 mm spacer thickness, followed by the type with discrete channels with 0.5 mm spacer thickness, while the flat bed had the lowest contribution to band variance.

When the printed device with the 0.1 mm thick spacers was cut open and inspected, it was observed that the spacers were not completely straight. This imperfection is suspected to be the cause of the discrepancy between computational and experimental testing. More extensive experimentation with different designs and possibly different 3D-printing techniques will be required to advance the technology.

3.2.2. Pressure limit of the devices

In pressure-driven liquid chromatography, a high-pressure resistance is desired for successful operation of a device. For our printed devices (Fig. 8) we aimed to determine the weakest points in the design (*i.e.* the points most prone to failure) and the pressure at failure in relation to the wall thickness. An initial encasing with wall thickness of 2 mm was chosen. In this case the device appeared most vulnerable near the outlet connection and the pressure at failure was about 1 MPa.

An increase of the encasing thickness to 5 mm was then realized, with the wall covering the surface of the outlet connector. The flow rate in the devices was raised step-wise until failure or up to a flow rate of 3 mL/min. The average maximum pressure was 3.5 MPa. In the majority of tests failure of the device was not encountered,

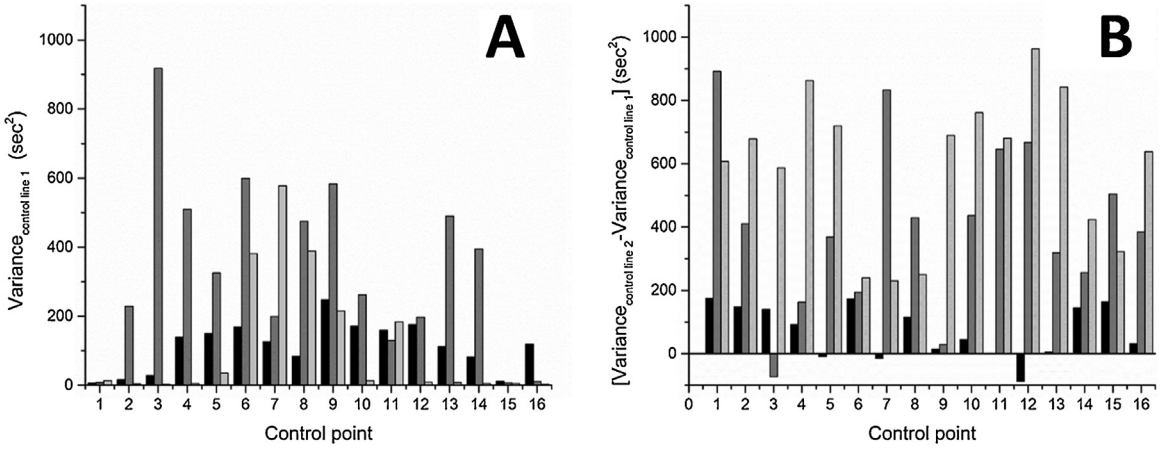

Fig. 7. A) Variance at the starting control line per point. B) Difference in variance between the ending and starting control lines per point. Black corresponds to the case with no spacers in the ^{2}D, grey to the case with spacers of 0.5 mm thickness and light grey to the case with spacers of 0.1 mm thickness.

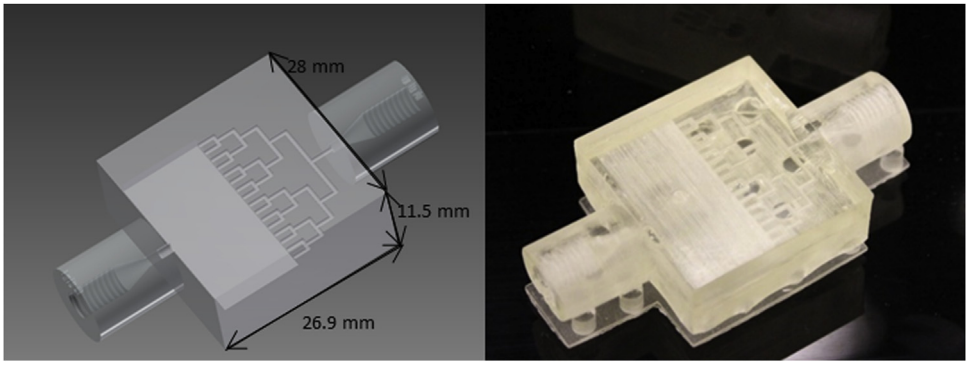

Fig. 8. Device used during pressure testing, consisting of a distributor, a flat bed and an outlet connector. In this case the top and bottom wall-thickness of 5 mm is used.

apart from the method with the steepest increase (increment of 1.5 mL/min instead of 1 mL/min in other cases), in which case failure occurred at approximately 4.5 MPa. However, some leakage around the connections was present in the majority of the cases at pressures exceeding 3 MPa.

The pressure tests indicate that the devices printed with a regular commercial photopolymer (*i.e.* not designed for maximal tensile strength) can operate at moderate pressures. High pressures used in column-based HPLC and UHPLC are not necessary for achieving high peak capacities spatial multi-dimensional separation [22]. If necessary, the pressure limit of the chips can be increased by using thicker walls, other photopolymers or external structural supports for the device. However, these results point to the ongoing challenge of developing pressure-resistant, low-dispersion fittings to 3D-printed polymer devices.

4. Conclusion and outlook

Two aspects of prospective two-dimensional spatial separation devices were studied, *viz.* efficient analyte transfer from the first (^{1}D) to the second (^{2}D) dimension and band broadening in the ^{2}D area of the device. Ten types of devices were studied using computational fluid dynamics (CFD) and initial experiments were performed on a selection of devices.

The presence of a stationary phase in the ^{1}D channel was found to have a dramatic effect on the efficiency of analyte transfer from ^{1}D to ^{2}D. Without a stationary-phase material present, a significant amount of the dye used to mimic analytes present in the ^{1}D channel remained in near-stagnant dead zones long after transfer was meant to be completed. As a result, injection bands in the second dimension showed a high variance and excessive tailing. To further explore the effects of dead zones in ^{1}D channels without a stationary material present, the diameter of the channels in the ^{2}D flow distributor was varied. Analyte losses were found to decrease upon increasing the diameter of the distributor flow channels.

CFD calculations suggested that the presence of spacers in the ^{2}D area would increase band dispersion. In the case of a ^{1}D channel with stationary material present, the ^{2}D band dispersion was found to increase with increasing spacer thickness, while in the cases with an empty ^{1}D channel this trend was not observed.

The contributions of spacers to the band dispersion in the ^{2}D area and the pressure limit of the fabricated devices were studied experimentally in devices created by high-resolution 3D-printing. A design without spacers was found to exhibit the lowest variance, in accordance with the CFD study. Thick (0.5 mm) spacers were found to perform better than thin (0.1 mm spacers), but this may be due to imperfections in the printed devices. Understandably, the thickness of the encasing of devices was found to significantly affect the pressure limit of 3D-printed devices. When increasing the encasing thickness from 2 mm to 5 mm the pressure at failure was found to increase from 1 to 4.5 MPa, although some leakage was observed around the connectors at pressures of about 3 MPa. The pressure limit may be improved with the use of an external holder and improved connectors will need to be studied.

The present study has contributed to progress in two-dimensional spatial chromatography. Suitable devices can, in principle, be created using 3D-printing and the knowledge created in the present study should contribute to the realization of successful devices in the near future.

Acknowledgements

The authors would like to acknowledge Noor Abdulhussain for her contributions to the pressure testing, Liana S. Roca for her assistance during flow testing and Bob W.J. Pirok and Alan Rodrigo García Cicourel for assisting in organizing the necessary laboratory equipment for the realization of the flow tests.

The STAMP project is funded under Horizon 2020-Excellent Science-European Research Council (ERC), Project 694151. The sole responsibility of this publication lies with the authors. The European Union is not responsible for any use that may be made of the information contained therein.

Sander Deridder gratefully acknowledges a research grant from the Research Foundation – Flanders (FWO-Vlaanderen).

Appendix A. Supplementary data

Supplementary material related to this article can be found, in the online version, at doi:https://doi.org/10.1016/j.chroma.2019.03.041.

References

[1] B.W.J. Pirok, D.R. Stoll, P.J. Schoenmakers, Recent developments in two-dimensional liquid chromatography – fundamental improvements for practical applications, Anal. Chem. 91 (2018) 240–263, http://dx.doi.org/10.1021/acs.analchem.8b04841.
[2] M. Gao, D. Qi, P. Zhang, C. Deng, X. Zhang, Development of multidimensional liquid chromatography and application in proteomic analysis, Expert Rev. Proteom. 7 (2010) 665–678, http://dx.doi.org/10.1586/epr.10.49.
[3] A. D'Attoma, S. Heinisch, On-line comprehensive two dimensional separations of charged compounds using reversed-phase high performance liquid chromatography and hydrophilic interaction chromatography. Part II: application to the separation of peptides, J. Chromatogr. A 1306 (2013) 27–36, http://dx.doi.org/10.1016/j.chroma.2013.07.048.
[4] X. Zhang, A. Fang, C.P. Riley, M. Wang, F.E. Regnier, C. Buck, Multi-dimensional liquid chromatography in proteomics-a review, Anal. Chim. Acta 664 (2010) 101–113, http://dx.doi.org/10.1016/j.aca.2010.02.001.
[5] A. Van Der Horst, P.J. Schoenmakers, Comprehensive two-dimensional liquid chromatography of polymers, J. Chromatogr. A 1000 (2003) 693–709, http://dx.doi.org/10.1016/S0021-9673(03)00495-3.
[6] P. Schoenmakers, P. Aarnoutse, Multi-dimensional separations of polymers, Anal. Chem. 86 (2014) 6172–6179, http://dx.doi.org/10.1021/ac301162b.
[7] E. Uliyanchenko, S. Van Der Wal, P.J. Schoenmakers, Challenges in polymer analysis by liquid chromatography, Polym. Chem. 3 (2012) 2313, http://dx.doi.org/10.1039/c2py20274c.
[8] T. Beelders, K.M. Kalili, E. Joubert, D. de Beer, A. de Villiers, Comprehensive two-dimensional liquid chromatographic analysis of rooibos (Aspalathus linearis) phenolics, J. Sep. Sci. 35 (2012) 1808–1820, http://dx.doi.org/10.1002/jssc.201200060.
[9] K.M. Kalili, A. de Villiers, Off-line comprehensive two-dimensional hydrophilic interaction x reversed phase liquid chromatographic analysis of green tea phenolics, J. Sep. Sci. 33 (2010) 853–863, http://dx.doi.org/10.1002/jssc.200900673.
[10] C.M. Willemse, M.A. Stander, J. Vestner, A.G.J. Tredoux, A. De Villiers, Comprehensive two-dimensional hydrophilic interaction chromatography (HILIC) × reversed-phase liquid chromatography coupled to high-resolution mass spectrometry (RP-LC-UV-MS) analysis of anthocyanins and derived pigments in red wine, Anal. Chem. 87 (2015) 12006–12015, http://dx.doi.org/10.1021/acs.analchem.5b03615.
[11] X. Ouyang, P. Leonards, J. Legler, R. van der Oost, J. de Boer, M. Lamoree, Comprehensive two-dimensional liquid chromatography coupled to high resolution time of flight mass spectrometry for chemical characterization of sewage treatment plant effluents, J. Chromatogr. A 1380 (2015) 139–145, http://dx.doi.org/10.1016/j.chroma.2014.12.075.
[12] B.W.J. Pirok, A.F.G. Gargano, P.J. Schoenmakers, Optimizing separations in on-line comprehensive two-dimensional liquid chromatography, J. Sep. Sci. 41 (2017) 68–98, http://dx.doi.org/10.1002/jssc.201700863.
[13] J.C. Giddings, Sample dimensionality: a predictor of order-disorder in component peak distribution in multidimensional separation, J. Chromatogr. A. 703 (1995) 3–15, http://dx.doi.org/10.1016/0021-9673(95)00249-M.
[14] G. Groeneveld, M.N. Dunkle, M. Rinken, A.F.G. Gargano, A. de Niet, M. Pursch, E.P.C. Mes, P.J. Schoenmakers, Characterization of complex polyether polyols using comprehensive two-dimensional liquid chromatography hyphenated to high-resolution mass spectrometry, J. Chromatogr. A 1569 (2018) 128–138, http://dx.doi.org/10.1016/j.chroma.2018.07.054.
[15] G. Guiochon, M.F. Gonnord, A. Siouffi, M. Zakaria, Study of the performances of thin-layer chromatography. VII. Spot capacity in two-dimensional thin-layer chromatography, J. Chromatogr. A. 250 (1982) 1–20, http://dx.doi.org/10.1016/S0021-9673(00)95205-1.
[16] J.C. Giddings, Two-dimensional separations: concept and promise, Anal. Chem. 56 (2007) 1258A–1270A, http://dx.doi.org/10.1021/ac00276a003.
[17] K.S. Mriziq, G. Guiochon, Column properties and flow profiles of a flat, wide column for high-pressure liquid chromatography, J. Chromatogr. A 1187 (2008) 180–187, http://dx.doi.org/10.1016/j.chroma.2008.02.037.
[18] G. Guiochon, N. Marchetti, K. Mriziq, R.A. Shalliker, Implementations of two-dimensional liquid chromatography, J. Chromatogr. A 1189 (2008) 109–168, http://dx.doi.org/10.1016/j.chroma.2008.01.086.
[19] C. Das, J. Zhang, N.D. Denslow, Z.H. Fan, Integration of isoelectric focusing with multi-channel gel electrophoresis by using microfluidic pseudo-valves, Lab Chip 7 (2007) 1806–1812, http://dx.doi.org/10.1039/b712794d.
[20] J. Liu, S. Yang, C.S. Lee, D.L. DeVoe, Polyacrylamide gel plugs enabling 2-D microfluidic protein separations via isoelectric focusing and multiplexed sodium dodecyl sulfate gel electrophoresis, Electrophoresis 29 (2008) 2241–2250, http://dx.doi.org/10.1002/elps.200700608.
[21] G. Guiochon, L.A. Beaver, M.F. Gonnord, A.M. Siouffi, M. Zakaria, Theoretical investigation of the potentialities of the use of a multidimensional column in chromatography, J. Chromatogr. A 255 (1983) 415–437, http://dx.doi.org/10.1016/S0021-9673(01)88298-4.
[22] E. Davydova, P.J. Schoenmakers, G. Vivó-Truyols, Study on the performance of different types of three-dimensional chromatographic systems, J. Chromatogr. A 1271 (2013) 137–143, http://dx.doi.org/10.1016/j.chroma.2012.11.043.
[23] B. Wouters, E. Davydova, S. Wouters, G. Vivo-Truyols, P.J. Schoenmakers, S. Eeltink, Towards ultra-high peak capacities and peak-production rates using spatial three-dimensional liquid chromatography, Lab Chip. 15 (2015) 4415–4422, http://dx.doi.org/10.1039/C5LC01169H.
[24] J.P. Grinias, R.T. Kennedy, Trends in analytical chemistry advances in and prospects of microchip liquid chromatography, Trends Anal. Chem. 81 (2016) 110–117, http://dx.doi.org/10.1016/j.trac.2015.08.002.
[25] E. Davydova, S. Wouters, S. Deridder, G. Desmet, S. Eeltink, P.J. Schoenmakers, Design and evaluation of microfluidic devices for two-dimensional spatial separations, J. Chromatogr. A 1434 (2016) 127–135, http://dx.doi.org/10.1016/j.chroma.2016.01.003.
[26] E. Davydova, S. Deridder, S. Eeltink, G. Desmet, P.J. Schoenmakers, Optimization and evaluation of radially interconnected versus bifurcating flow distributors using computational fluid dynamics modelling, J. Chromatogr. A 1380 (2015) 88–95, http://dx.doi.org/10.1016/j.chroma.2014.12.063.
[27] S. Jespers, S. Deridder, G. Desmet, A microfluidic distributor combining minimal volume, minimal dispersion and minimal sensitivity to clogging, J. Chromatogr. A 1537 (2018) 75–82, http://dx.doi.org/10.1016/j.chroma.2018.01.029.
[28] H.K. Versteeg, W. Malalasekra, An Introduction to Computational Fluid Dynamics: the Finite Volume Method, Pearson Education Ltd., Harlow, England, 2007.
[29] R. Taylor, R. Krishna, Multicomponent Mass Transfer, Wiley, 1993.
[30] P. Gzil, N. Vervoort, G.V. Baron, G. Desmet, Advantages of perfectly ordered 2-D porous pillar arrays over packed bed columns for LC separations: a theoretical analysis, Anal Chem. 75 (2003) 6244–6250, http://dx.doi.org/10.1021/ac034345m.
[31] J. Liu, C.F. Chen, S. Yang, C.C. Chang, D.L. DeVoe, Mixed-mode electrokinetic and chromatographic peptide separations in a microvalve-integrated polymer chip, Lab Chip 10 (2010) 2122–2129, http://dx.doi.org/10.1039/c003505j.
[32] B. Wouters, J. De Vos, G. Desmet, H. Terryn, P.J. Schoenmakers, S. Eeltink, Design of a microfluidic device for comprehensive spatial two-dimensional liquid chromatography, J. Sep. Sci. 38 (2015) 1123–1129.
[33] S. Deridder, S. Eeltink, G. Desmet, Computational study of the relationship between the flow resistance and the microscopic structure of polymer monoliths, J. Sep. Sci. 34 (2011) 2038–2046, http://dx.doi.org/10.1002/jssc.201100220.
[34] T. Adamopoulou, S. Deridder, G. Desmet, P.J. Schoenmakers, Two-dimensional insertable separation tool (twist) for flow confinement in spatial separations, J. Chromatogr. A 1577 (2018) 120–123, http://dx.doi.org/10.1016/j.chroma.2018.09.054.